ISPRS Journal of Photogrammetry and Remote Sensing 109 (2015) 108–125

Contents lists available at ScienceDirect

ISPRS Journal of Photogrammetry and Remote Sensing

journal homepage: www.elsevier.com/locate/isprsjprs

A robust mosaicking procedure for high spatial resolution remote sensing images

Xinghua Li [a,1], Nian Hui [b,1], Huanfeng Shen [a,c,*], Yunjie Fu [d], Liangpei Zhang [c,e]

[a] School of Resource and Environmental Sciences, Wuhan University, Wuhan, Hubei province, China
[b] Department of Navigation Data, Wuhan Kotei Informatics Co., Ltd., Wuhan, Hubei province, China
[c] Collaborative Innovation Center for Geospatial Information Technology, Wuhan University, China
[d] Chongqing Institute of Surveying and Mapping, NASM, Chongqing, China
[e] State Key Laboratory of Information Engineering in Surveying, Mapping, and Remote Sensing, Wuhan University, Wuhan, Hubei province, China

ARTICLE INFO

Article history:
Received 15 November 2014
Received in revised form 17 September 2015
Accepted 21 September 2015

Keywords:
Cosine distance weighted blending
Image mosaicking
High spatial resolution
Local moment matching
Piecewise dynamic program
Remote sensing

ABSTRACT

With the rapid development of sensor manufacturing technology, high spatial resolution (HR) images are becoming more easily acquired and more widely used. However, it is common that a region of interest (ROI) cannot be completely acquired from a single image. Image mosaicking can resolve the problem by creating a new large-area image from multiple images with overlapping areas. A typical mosaicking procedure for HR remote sensing images includes three successive steps: tonal adjustment, seamline detection, and image blending. In this paper, we propose a robust mosaicking procedure featuring novel ideas in all three steps, which is aimed at processing HR remote sensing images of urban areas. Firstly, the tonal adjustment is realized by a local moment matching (LMM) algorithm, which solves the nonlinear photometric correlation problem between adjacent images. Secondly, an automatic piecewise dynamic program (APDP) algorithm for seamline detection is proposed to detect the optimal seamline on the overlapped area. Last but not least, we propose a cosine distance weighted blending (CDWB) method to ensure that the seamline is as invisible as possible. Compared to the state-of-the-art methods, the proposed method was proved to be effective in experiments with high resolution aerial and satellite images.

1. Introduction

In the last decades, high spatial resolution (HR) remote sensing images have become widely used to embody abundant geographic information. However, the narrow geographic range within a single image is one of the main factors which limits the further application of HR images. As we know, in terms of images with the same size, the higher the spatial resolution, the narrower the geographic range. As a result, the region of interest (ROI) often cannot be included in a single image. How to acquire a complete ROI from HR images has always been a hot topic. Accordingly, image mosaicking has been developed to solve the problem. In a nutshell, image mosaicking is the process of merging two or more images with overlapping areas into a single view with an indistinguishable seamline (Burt and Adelson, 1983).

Briefly speaking, there are two main reasons for the difficulties encountered in remote sensing image mosaicking. One is that the images are often taken at different times, and the other is that they are often taken from different angles. The former issue leads to different geographic features existing on the overlapped area, and a big tonal difference. The latter issue causes shape differences in the same geographic features on the overlapped area, especially for HR images. In other words, when the camera takes images from different angles, different objects will appear in the same position according to the geographic reference. To this end, the current mosaicking procedures for remote sensing images are structured as follows. Firstly, in order to make the mosaicked image a natural integrated image, tonal adjustment is necessary. A fusion process should then be undertaken. In general, the images to be mosaicked must have overlapping areas (shared areas). After the tonal adjustment, averaging the pixels of the overlapped area is the simplest way to mosaic the images. For low spatial resolution images, this

* Corresponding author at: School of Resource and Environmental Sciences, Wuhan University, Wuhan, Hubei province, China.
E-mail address: shenhf@whu.edu.cn (H. Shen).
[1] These authors contributed equally to this study and shared first authorship.

http://dx.doi.org/10.1016/j.isprsjprs.2015.09.009
0924-2716/

method is very effective. However, when it comes to HR remote sensing images, this approach may cause ghosting. Researchers have therefore investigated how to find an appropriate seamline to weaken the ghosting effect (Chon and Kim, 2006). When an optimal seamline is detected, pixels of the mosaicked image approximately rely on only one image, based on which side of the seamline they lie on (Pan et al., 2009). A blending algorithm is also necessary to reduce the residual differences between the two neighboring images in a buffer along the seamline (Chon and Kim, 2006). To sum up, three successive steps are required to generate a satisfactory mosaicked image from HR images: tonal adjustment, seamline detection, and image blending.

In this study, we propose a robust mosaicking procedure for HR images, with the following improvements in tonal adjustment, seamline detection, and image blending. Note that the HR images to be mosaicked all have overlapping areas. In the first step, the tonal differences are corrected by local moment matching (LMM). An automatic piecewise dynamic program (APDP) seamline detection method then determines the location of the optimal seamline in the overlapped area. In the final step, the seamline is eliminated by a new method of cosine distance weighted blending (CDWB).

The rest of this paper is organized as follows. In Section 2, we survey the current approaches to image mosaicking. The algorithms we propose in this paper are discussed in Section 3, which is followed by the mosaicking experiments in Section 4. The conclusions and discussions are drawn in Section 5.

2. Related works

As was previously mentioned, there are three key aspects in image mosaicking: tonal adjustment, seamline detection, and image blending. In this section, we introduce some of the existing methods for these three aspects.

2.1. Tonal adjustment

Tonal adjustment plays an important role in making a mosaicked image appear to be a natural single image. The current approaches to tonal adjustment are based on the premise that the reflection conditions in the overlapped region remain constant. The average luminance condition of the reference image in the overlapped area is computed, and the other image is normalized into uniformity (Du et al., 2001). The mean value denotes the average of the image intensity, and the variance or standard deviation represents the volatility of the intensity. These are the most basic indicators for image tone. Yi et al. (2003) detailed three common tonal adjustment methods: (1) the approaches based on image entropy; (2) the methods using mean variance; and (3) histogram matching. The approaches based on entropy are based on the principle that the overlapping areas of the adjacent images represent the same area, so the entropy should also be the same. The color difference is then eliminated by entropy mapping. The methods based on mean variance adjust the tone using the mapping relationship between the image mean and variance (Zhang et al., 2003). Histogram matching stretches the histogram of all the bands in one image to be similar to the shape of the reference image, to adjust the tone (Du et al., 2001; Gonzalez and Woods, 2007). Mills and Dudek (2009) used a linear approximation model to adjust the tone generally. These kinds of methods compute a pair of gain and bias values based on the overlapped area, and build a linear correlation of the image before and after adjustment (Zhang et al., 2003; Gonzalez and Woods, 2007). This sort of adjustment has the common shortcoming that the image may appear dark or bright in the overall view. In this case, some local features in the tone may be ignored. To avoid the overall luminance difference and to allow better consideration of the local features, we propose the LMM algorithm in the step of tonal adjustment.

2.2. Seamline detection

As to the detection of the seamline, this has always been the focus of HR image mosaicking (Zagroub et al., 2009). Seamline detection aims at finding the optimal seamline where the images share the most similarity. When detecting the seamline in an urban area with clusters of buildings, if the seamline can go through a flat area, or go along the natural edges of the buildings, instead of crossing the buildings, it will be hidden among these complex geographic entities (Duplaquet, 1998).

Based on the snake model (Kass et al., 1988), Wang et al. proposed the improved snake model (Wang et al., 2010). In their work, the sum of the mismatched values on the line is considered as the energy. The line with the lowest energy is then the optimal seamline. This model solves the local optimum problem existing in the snake model, to some extent, but not completely. Kerschner (2001, 2000) proposed the twin snake algorithm. In this approach, the two lines of the twin snake start from opposite borders of the overlapped area, and are forced to be attracted to each other. The optimal seamline is determined if the two lines are merged. However, this algorithm cannot overcome the local minima problem completely, and it requires a high computational cost (Chon and Kim, 2006).

Dijkstra (1959) proposed Dijkstra's algorithm to solve the problem of the shortest path, and Davis (1998) used this algorithm to choose the optimal seamline for images with moving objects. In this approach, the seamline is placed by creating a difference image for the two neighboring images, with pixels given higher values if they have greater intensity differences. The optimal seamline is then the minimum cost path from one edge of the overlapped area to the other. Unfortunately, the algorithm has two shortcomings: it is only useful for carefully controlled source images, and its traversal efficiency is a little low for remote sensing images.

Pan et al. (2009) proposed large-area Voronoi diagrams to generate a seamline network for mosaicking over a large geographic area. This algorithm, which can easily obtain a seamline network, especially for multi-image mosaicking, is suitable for common industrial production. However, for high-accuracy mosaicking, this method cannot fulfill the requirements.

Duplaquet (1998) developed a dynamic program (DP) based algorithm combining the color and gradient similarity to trace the optimal seamline. The DP algorithm (Agrawal and Horgan, 1990) is also an algorithm that can obtain the shortest path. However, compared with Dijkstra's algorithm, the time consumption is much less. The most significant superiority of the DP algorithm is the rapid operation, which is very important for HR remote sensing image mosaicking. However, the accuracy of the seamline location by the use of the DP algorithm still has room for improvement. Xing et al. (2010) used an algorithm modified from the DP algorithm, which showed a slight improvement over the original DP algorithm. Nevertheless, the detected seamline still easily goes through buildings, which causes obvious discontinuity. To avoid such discontinuity, we propose the APDP algorithm in this paper.

2.3. Image blending

The third step—image blending, also called feathering (Levin et al., 2004)—provides a smooth transition near the seamline. In this field, hard correction (HC) (Zhu and Qian, 2002; Shmuel, 1981), weighted stacking on overlapped areas (Chon and Kim, 2006; Gonzalez and Woods, 2007; Uyttendaele et al., 2001), and

wavelet transform (Zhu and Qian, 2002) are the most common approaches. For HC, the intensity difference at both sides of the seamline is calculated, and it is then reallocated to the statistical area from one side to the other side so that the transition is natural. If the path of the seamline is horizontal, it will be eliminated vertically; whereas, if the seamline is vertical, it will be corrected horizontally. When the exposure difference is quite obvious, HC cannot effectively realize a smooth transition. The stacking method, as is implied by the name, replaces the values along the seamline with the sum of several original images with different weights (Kang, 2006). For instance, for pixels on the left of the seamline, the image on the left has a higher weight, and vice versa. Sometimes the original images have only a small overlapped area, or the images are not registered to a high degree of accuracy. In this case, the stacking method may lead to ghosting. Wavelet transform is a new approach developed in recent years. In its framework, images are broken down into wavelet components with different frequencies, which are mosaicked at different scales. Finally, the mosaicked image is retrieved with an algorithm which has a very strict theoretical basis. This approach is, however, complex to compute. In order to realize a more natural transition, we propose a simple CDWB method, which is also a kind of stacking method.

3. Algorithms

The proposed algorithms for the mosaicking of HR images are shown in Fig. 1. It should be explained that in this whole paper, we only consider the mosaicking of two images. One of the two images is on the left, and the other is on the right. The procedure is similar to mosaicking two images with other relative positions. Firstly, based on the overlapped area, the tonal difference is corrected with LMM. After that, APDP is used to find an optimal seamline on the overlapped area. The two images are then mosaicked into a single image along the seamline. In this step, CDWB is utilized on a buffer along the seamline to eliminate the seamline and generate a smooth transition. In terms of the three steps of HR image mosaicking—tonal adjustment, seamline detection, and image blending—they are described in detail as follows.

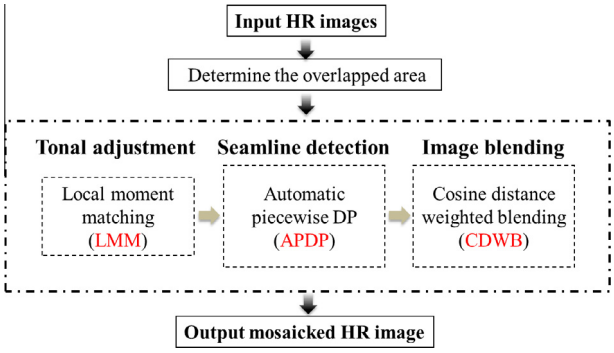

Fig. 1. Flowchart of the proposed method for the mosaicking of HR images.

3.1. Tonal adjustment using LMM

In this part, we present a tonal adjustment method, namely LMM, to solve the nonlinear photometric correlation problem between the adjacent images to be mosaicked. Based on the overlapped region, least squares matching (LSM) (Pham and Pringle, 1995), mean–variance matching (Yi et al., 2003; Zhang et al., 2003), and moment matching (MM) (Zhong et al., 2006) are methods which adjust the tone using only a pair of gain and bias values based on the whole image. The overall tonal adjustment for large-area images with only one pair of gain and bias values ignores the local tonal differences and can lead, on the whole, to darkness or brightness. For a better consideration of the regional tonal differences, and to avoid overall luminance deviation, we propose to adjust the tone of different successive regions with different pairs of gain and bias values. Generally speaking, the proposed tonal adjustment method performs better than the methods which use only one pair of gain and bias values for the whole image. For brevity, we take the improved method based on the traditional MM as an example, i.e., the aforementioned LMM. It is introduced in detail in the following.

Fig. 2 illustrates tonal adjustment using LMM. The overlapped region in image g is the reference, and f is the image to be corrected. Let $f(i,j)$ and $\hat{f}(i,j)$ denote the pixel values in row i, column j of the image f and the corrected image, respectively. A region is a rectangular area composed of the rows from $i-R$ to $i+R$ (R is a constant parameter which influences the effect of the tonal adjustment), moving with the change of i (e.g., Region a_i and Region b_i). A_i and B_i are the gain and bias values calculated in Region a_i and Region b_i, respectively. The pair of A_i and B_i is then used to adjust the tone of row i in image f as follows:

$$\hat{f}(i,j) = A_i \cdot f(i,j) + B_i \tag{1}$$

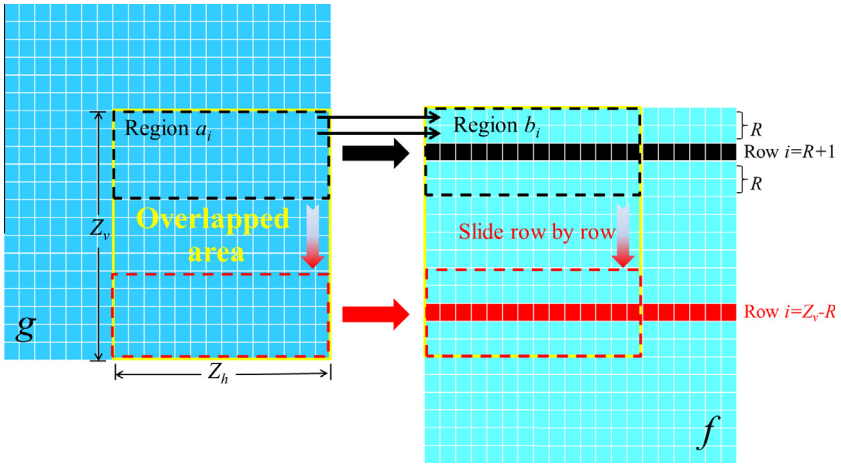

Fig. 2. Tonal adjustment using LMM.

where on the overlapped area

$$A_i = \frac{\delta_{g(i)}}{\delta_{f(i)}}, \qquad B_i = M_{g(i)} - M_{f(i)} \times A_i \quad (R < i \leqslant Z_v - R) \tag{2}$$

where $\delta_{g(i)}$ and $\delta_{f(i)}$ are the standard deviations of Region a_i and Region b_i, respectively, and $M_{g(i)}$ and $M_{f(i)}$ are the corresponding averages. Additionally, Z_v is the height of the overlapped area, and row $Z_v - R$ is the middle row in the region nearest to the end of the overlapped area, as shown in Fig. 2.

In other words, instead of adjusting the overall tone using MM, LMM adjusts image f row by row. The coefficients calculated between Region a_i and Region b_i are used to correct row i in image f. With the joint moving of Region a_i and Region b_i, row by row, the whole image f is gradually corrected. Note that the first few rows $(1 \leqslant i \leqslant R)$ in image f are adjusted based on the regions centered at row i on the overlapped area of the two images. The last rows $(i \geqslant Z_v - R)$ in image f are adjusted based on the regions centered at row $Z_v - R$ in the two images. This region-based adjustment algorithm allows for the consideration of the local tonal characteristics of a large-area image. It not only makes sure that the final mosaicked image is a single-entity view, but also lays a solid foundation for the subsequent blending process. Furthermore, it can be applied to other traditional overall-adjustment methods, such as LSM, mean–variance matching, and so on. The tonal adjustment also contributes to the detection of an optimal seamline, which is verified in the experiments.

3.2. Seamline detection using APDP

Generally speaking, seamline detection is the most important step in the procedure. As described earlier, mosaicking two images along a poor seamline will cause obvious artificial frontiers. A good seamline should go through the most similar parts of the original images, to result in the least discontinuity. There are two possible circumstances for an invisible seamline: going through radiometrically exactly equal areas, or following the natural edges of geographic entities common to both images. Based on the current research, we propose the APDP method to detect the optimal seamline.

3.2.1. The process of APDP

In certain particular conditions, the seamline detected by non-piecewise methods may go through buildings and result in ghosting. To alleviate this phenomenon, we propose an auto piecewise seamline detection method based on DP: APDP. The mode of piecewise detection is the first difference between APDP and the current methods (DP and Dijkstra's algorithm). Since piecewise detection can control the deviation of the optimal seamline in each piece, it can avoid ghosting, and the total deviation of the optimal seamline will be decreased. As shown in Fig. 3, the optimal seamline is divided into many pieces to be detected (Piece I, Piece II, Piece III ...). The length of the seamline and the cost of detection are the two controlling factors for piecewise detection. Inside each piece, the longest seamline with the lowest average cost will be the

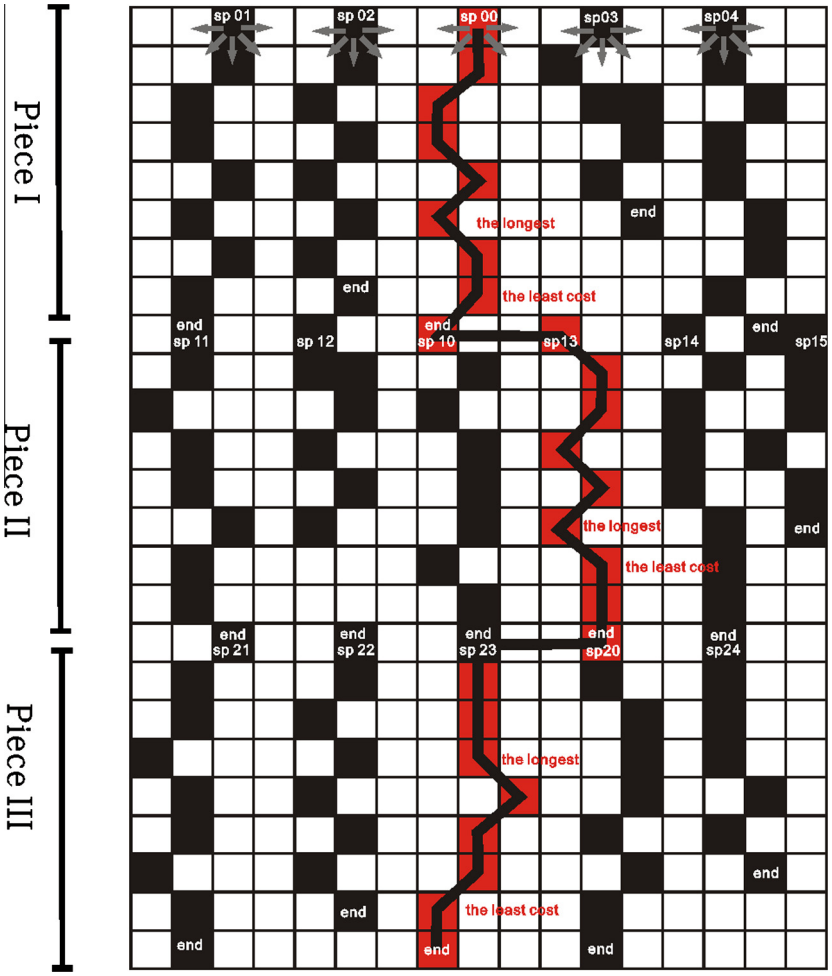

Fig. 3. Piecewise seamline detection using APDP.

optimal one. The end point of this piece of seamline will then decide the new starting point of the next piece of seamline. In Fig. 3, "sp" denotes the starting point of one piece of the seamline, and "end" represents the end of this piece. Pixel "sp∗0" (∗ means 1, 2, 3, ...) is the starting point of the local optimal seamline in the corresponding piece. We repeat this cycle until the seamline reaches the end of the overlapped area. All these pieces of seamline are then connected to become the optimal seamline.

3.2.2. The APDP algorithm

Duplaquet (1998) proposed the following requirements for an optimal seamline:

(1) On the seamline, the intensity difference of pixels in the two images is minimal.
(2) The geometric difference along the seamline is minimal.

These criteria are such that an ideal supposition in which a seamline simultaneously meets the two cases may not exist. Our objective is therefore to find the closest seamline to the ideal one. In order to find the optimal seamline, a cost function is set for each seamline. Among all the seamlines, the longest one with the lowest average cost is the optimal seamline.

Let N_s be the average cost of each piece of piecewise seamline starting from the overlapped area, and N_{op} and L_{op} denote the cost and the length of the optimal seamline, respectively. Taking the intensity difference, the geometric structure difference, and the gradient similarity of the images into consideration, we propose the following algorithm to detect the optimal piece of seamline:

$$\begin{aligned} N_s &= \sum_{k=1}^{L_s} \min\left(N^s_{dmk} + N^s_{emk} + N^s_{gmk}\right)/L_s (m = 0,1,2,3,4 \\ &\quad \text{and} \quad S = 1,\ 2,\ \ldots, Z_h) \\ N_{op} &= \min(N_s) \\ L_{op} &= \max(L_s) \end{aligned} \tag{3}$$

with

$$\begin{aligned} N_{dmk}(i_m, j_m) &= \frac{1}{(2X+1)(2Y+1)} \sum_{x=-X}^{X} \sum_{y=-Y}^{Y} |g(i_m + x, j_m + y) \\ &\quad - \hat{f}(i_m + x, j_m + y)| \\ N_{gmk}(i_m, j_m) &= Min\left(grad_g(i_m, j_m), grad_{\hat{f}}(i_m, j_m)\right) \\ N_{emk}(i_m, j_m) &= \sum_{t=1}^{8} |G_t(i_m, j_m)| \end{aligned} \tag{4}$$

with

$$G_t(i_m, j_m) = (g(i_m, j_m) - \hat{f}(i_m, j_m)) \times S_t \tag{5}$$

where the notations are as follows: m denotes the search direction, as shown in Fig. 4. As is shown in Fig. 4, point 5 is the current pixel on the seamline, and points 0–4 are the next candidate pixels of point 5 in the five search directions. Z_h is the width of the overlapped area, as shown in Fig. 2. L_s is the length (number of pixels) of a piece of piecewise seamline. $g(i,j)$ and $\hat{f}(i,j)$ are the intensities of images g and $\hat{f}$ with the coordinates of (i,j), respectively. For each pixel (i,j) on the seamline, it corresponds to a group of pixels (i_m, j_m) in the search directions. N_{dmk} denotes the intensity difference in a $(2X+1) \times (2Y+1)$ window around pixels 0–4. N_{gmk} represents the gradient similarity between the current pixel and the five adjacent pixels in the search directions. $Min(a,b)$ represents the smaller one between a and b. N_{emk} is the geometric structure difference around pixels 0–4. It is calculated by an eight-direction Sobel gradient operator (0°, 45°, 90°, 135°, 180°, 225°, 270°, 315°) which can detect the edge information. $G_t(i_m, j_m)$ is the Sobel gradient in one direction. S_t is the Sobel operator used in the eight directions (Xing et al., 2010). $a \times b$ represents the convolution of a and b. $grad_g$ and $grad_{\hat{f}}$ are the first-order gradients between the current pixel and the next candidate pixel in images g and $\hat{f}$.

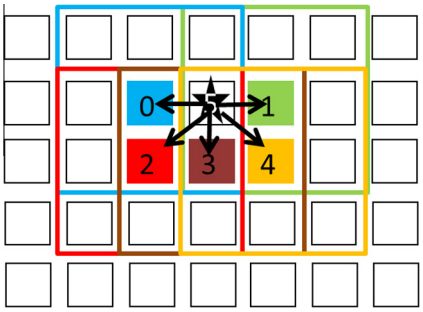

Fig. 4. Five search directions for a seamline in APDP. Point 5 is the pixel on the seamline.

In addition to the piecewise mode, APDP has two other differences with the original DP: (1) APDP searches in five directions instead of three directions (the directions of 2, 3, and 4 in Fig. 4) in the DP method; (2) DP only uses $N_{dmk} + N_{gmk}$, and does not include the geometric structure N_{emk}. The piecewise method is realized by the control of the length of each partial seamline and the cost threshold of $N_{dmk} + N_{emk} + N_{gmk}$ (Fig. 3). The formula $N_{dmk} + N_{emk} + N_{gmk}$ restrains the trend of the optimal seamline with regard to both geometric structure and intensity. The piecewise detection method is effective in controlling the seamline along flat areas, because once the seamline goes through a building, $N_{dmk} + N_{emk} + N_{gmk}$ will go beyond the threshold. Accordingly, the current piece of seamline will end and the next detection piece will start. The final optimal seamline is made up of many piecewise parts.

In fact, even if the final seamline is the optimal one, the top and bottom borders of the original images will be the artificial borders of the mosaicked image. To solve this problem, the final seamline is the one which starts from one angular vertex (top) of the overlapped area to another angular vertex (bottom). It is made up of three parts: the first part starts from the top vertex of the overlapped area; the second part is mostly in the longitudinal; and the third part starts from the bottom vertex of the overlapped area. The three parts are connected to be the final seamline with intersections. In fact, the specific searching direction is affected by the position relationship between the two neighboring images. Taking the left–right position as an example, there are four cases in Fig. 5. In this paper, our algorithms are presented as in Fig. 5(a).

APDP is detailed as follows (see Fig. 6):

(1) Set pixels $(1,i)$ in the first row of the overlapped area as the starting point of one seamline. Each point will start a seamline, and we choose the optimal one.
(2) Detect the seamline from these starting points to their corresponding five directions (as shown in Fig. 4) until the end of the overlapped area. Choose the longest one with the lowest average cost to be the initial selection of the optimal seamline. Record this starting point (c,u) and let it be the starting point in the piecewise detection.
(3) Choose 10 points (empirical number, it can be another number) on the left and right sides of (c,u) as new starting points and begin the piecewise detection. Each point will start a new piece. Once the cost (the sum of N_d, N_g, and N_e) of pixel (i_m, j_m) is beyond the threshold TL, or

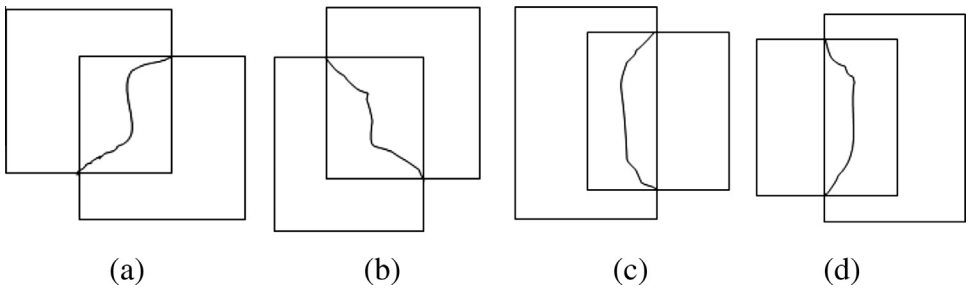

Fig. 5. The position relationships between two left–right relationship images. (a) Left-up and right-down. (b) Left-down and right-up. (c) Right-in-left. (d) Left-in-right.

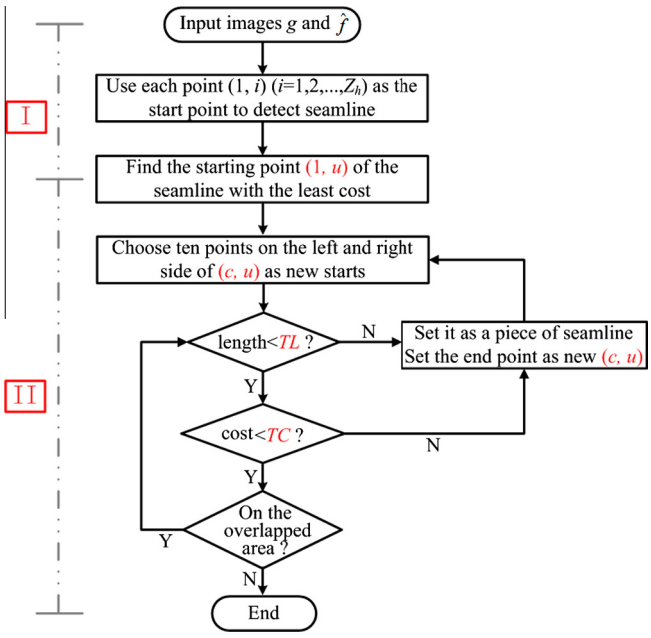

Fig. 6. The flowchart of optimal seamline detection using APDP.

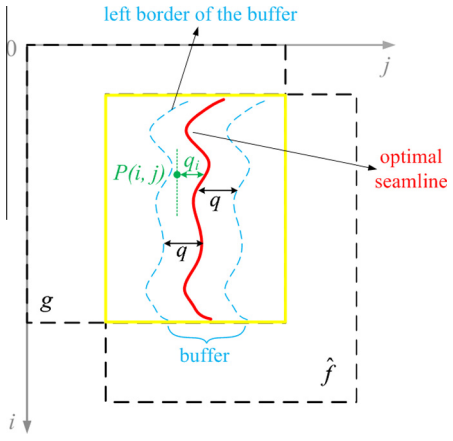

Fig. 7. Schematic diagram of the buffer in image blending.

the length of the present piece is beyond the threshold *TL*, this piece of seamline will be ended. In general, *TL* has a limited influence on the seamline detection. Although different values of *TL* obtain similar detection results, a smaller value of *TL* may result in trivial pieces. We suggest that $TL = 100$ is an appropriate setting. In contrast, *TC* has a more obvious impact on the seamline detection, which is discussed in the experimental section. We then choose the longest seamline in the 21 seamlines with the lowest average cost to be the optimal one. Following this, we set the end point of the optimal piece as the new center point to choose the starting points of a group of new pieces.

(4) Repeat step (3) until the end of the overlapped area. Connect these optimal pieces of seamline to be one integrated seamline (longitudinal seamline).

As was noted previously, to reduce the artificial borders of the original image, the final seamline consists of three parts. The previous steps detected a longitudinal seamline. Following the above steps, we detect seamlines towards the middle of the overlapped area from the two vertexes (up and down) of the overlapped area (according to Fig. 5). We let the two seamlines intersect with the

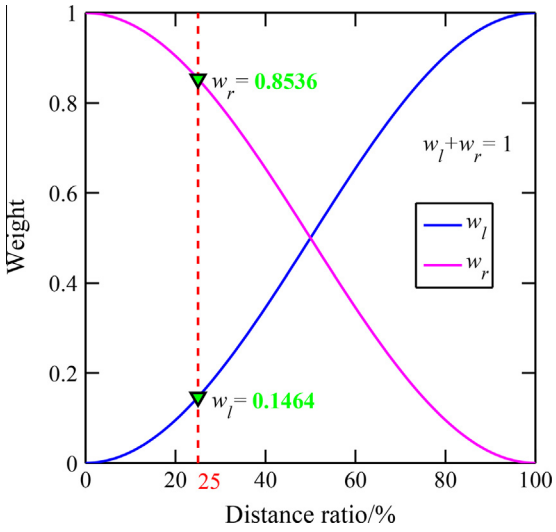

Fig. 8. Diagram showing how the weight varies with the distance ratio in image blending using CDWB.

Table 1
Experimental parameters setting of the three steps for the proposed method.

Steps	Parameters
Tonal adjustment	$R = 10$
Seamline detection	$TC = 250$
	$TL = 100$
Image blending	$q = 10$

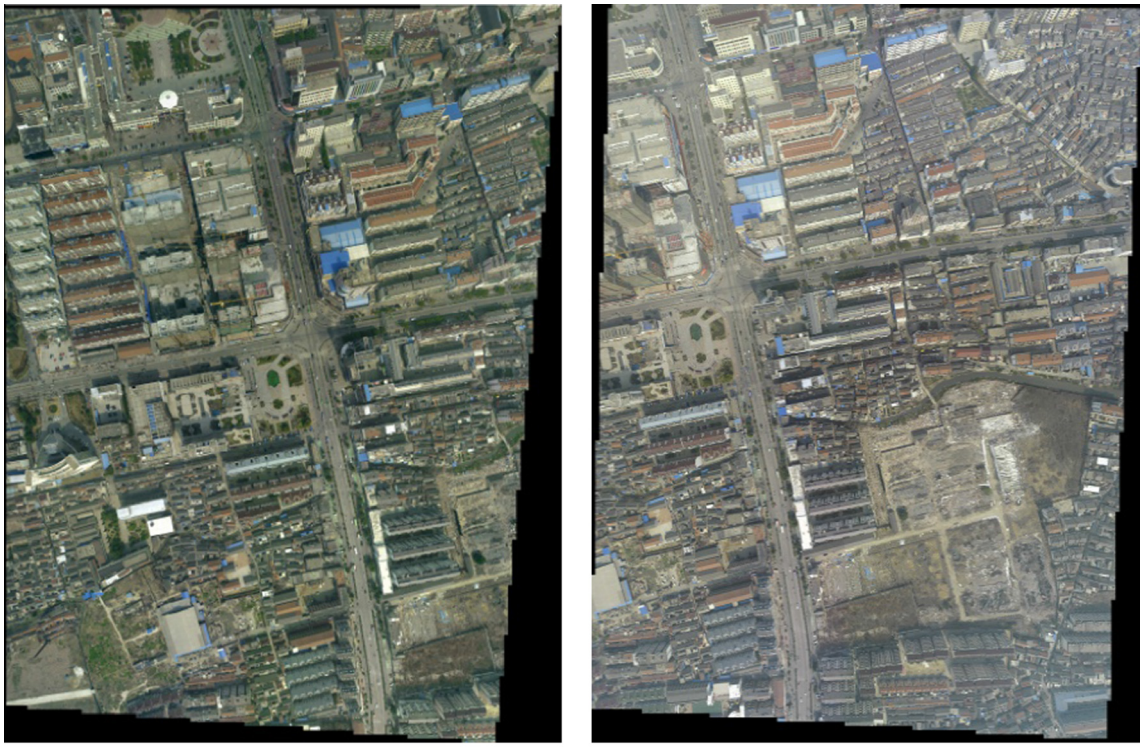

Fig. 9. The original HR images (the overlapped area of the two images is of a size of 4700 × 8300). (a) The left image (with the size of 6700 × 8900). (b) The right image (with the size of 6500 × 8800).

longitudinal seamline in step (4) and connect the three seamlines to be the final optimal seamline.

3.3. Image blending using CDWB

As the name implies, image blending is the process used to make the seamline invisible. In the following content, we explain the CDWB image blending method. Elimination of the seamline plays an important role in making a smooth transition. In CDWB, a buffer along the final seamline detected in Section 2 is set as a transition zone, as shown in Fig. 7. Outside the buffer, the left area of the mosaicked image comes from the left original image, and the right area comes from the right image; inside the buffer, each pixel value is a weighted combination of the corresponding overlapped pixels from the two images. We believe that appropriate weights are the guarantee of a smooth transition. To date, a number of different kinds of weighting methods have been used in the field of image processing. Without any loss of generality, we choose a simple weighting standard: distance. In other words, the shorter the distance, the greater the weight. For example, as shown in Fig. 7, for any pixel $P(i,j)$ in the buffer, the distance $q - q_i$ (where q is the half width of the buffer) is from the pixel to the left border of the buffer. The closer the pixel $P(i,j)$ lies to the left border of the buffer, the heavier the weight of the left image is, and the lighter the weight of the right image is; and vice versa. Let d be the distance ratio of $P(i,j)$ to the seamline, i.e.

$$d = \frac{q - q_i}{2q}, \quad -q \leqslant q_i \leqslant q \tag{6}$$

where q_i denotes the distance of $P(i,j)$ to the optimal seamline, as shown in Fig. 7. If $P(i,j)$ is on the left of the seamline, q_i is negative; if $P(i,j)$ is on the right, q_i is positive.

Concretely, suppose M is the final mosaicked image, i.e.

$$M(i,j) = \begin{cases} g(i,j), & (i,j) \in g \\ w_l(i,j) * g(i,j) + w_r(i,j) * \hat{f}(i,j) & (i,j) \in (g \cap \hat{f}) \\ \hat{f}(i,j), & (i,j) \in \hat{f} \end{cases} \tag{7}$$

where $w_l(i,j)$ and $w_r(i,j)$ are the respective weights of images g and $\hat{f}$ in the buffer. It is required that $w_l(i,j) + w_r(i,j) = 1$ and $0 \leqslant w_l(i,j), w_r(i,j) \leqslant 1$. In the framework of the traditional distance weighting method, because the transition of the weights close to the edge of the buffer (0 and 1) is not smooth, the blending effect may be poor in the border of the buffer. Here, the traditional method means inverse distance weighting (IDW) Fisher et al., 1987. Inspired by the way a cosine varies in the range $[0, 1]$ and changes very slowly at the ends of 0 and 1 (see Fig. 8), we propose a new weight calculation algorithm based on the cosine distance. Firstly, we suppose $w_l(i,j)$ and $w_r(i,j)$ are both the functions of the distance ratio d, and we let $w_l(d)$ substitute for $w_l(i,j)$ and $w_r(d)$ substitute for $w_r(i,j)$. To obtain reasonable weights, the following assumptions are made:

(1) We consider constant weight functions outside the buffer, and we want to have a differentiable mosaicking and consequently weight functions for a smooth transition. Therefore, at the borders of the buffer, the first derivatives need to be zero, i.e., $w_l'(1) = 0$, $w_r'(0) = 0$.
(2) At the borders of the buffer, the weight should be 0 or 1, i.e., $w_l(0) = 1$ and $w_r(0) = 0$ or $w_l(1) = 0$ and $w_r(1) = 1$.
(3) Inside the buffer, $w_l(d) + w_r(d) = 1$.

According to these principles, the following cosine-based formula is used to calculate $w_l(d)$ and $w_r(d)$. At first, $w_l(d)$ is calculated by:

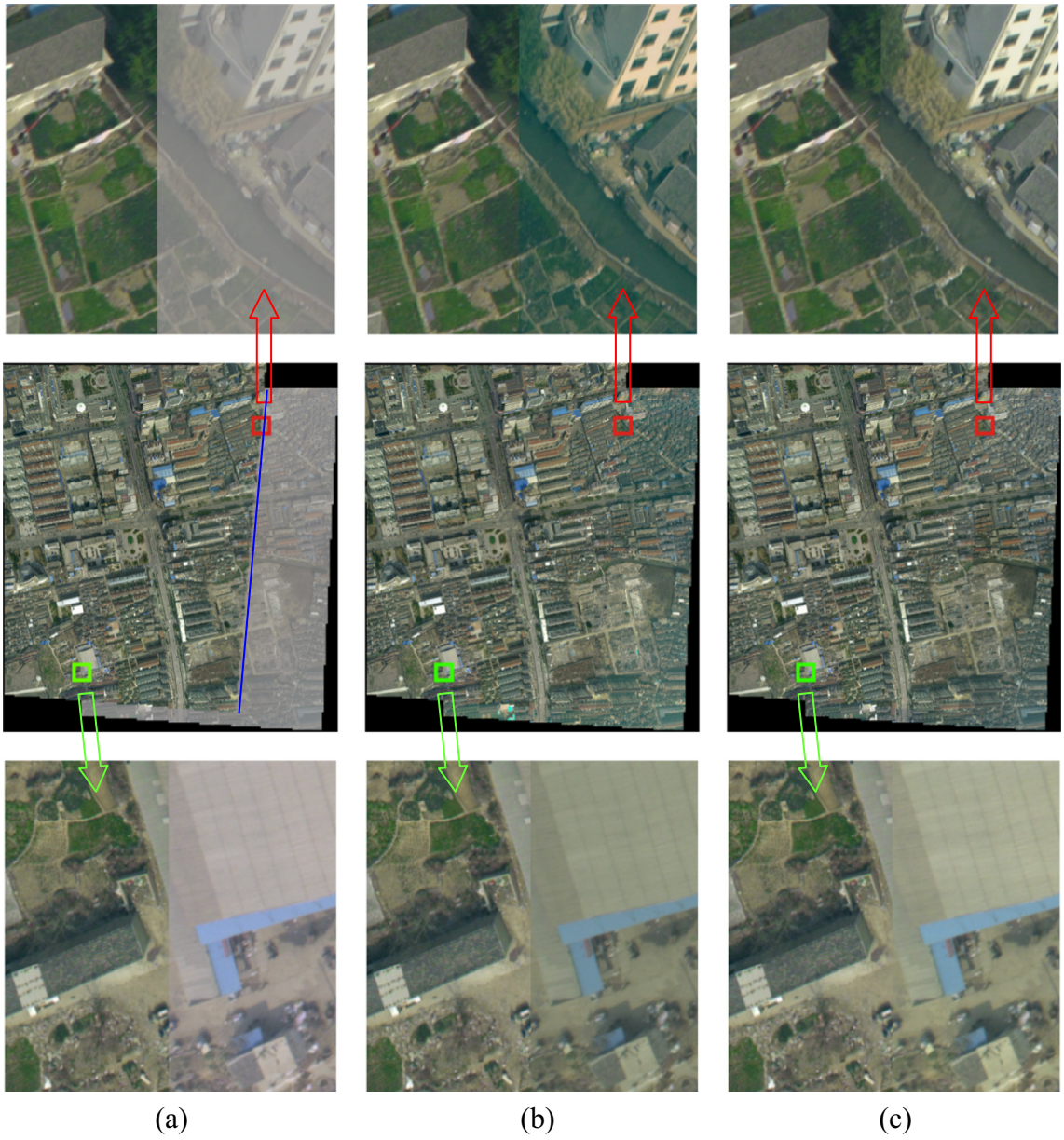

Fig. 10. Tonal adjustment results with the different methods. (a) The result of LSM. (b) The result of MM. (c) The result of the proposed LMM.

Table 2
The horizontal gradient at the color transition of the image to be mosaicked in Fig. 10.

Bands	Methods		
	LSM	MM	LMM
Red	44.8754	27.0704	**24.7488**
Green	35.8470	22.2306	**21.0377**
Blue	42.8686	20.7714	**18.8487**

Bold values are the best values of the three methods.

$$w_l(d) = \omega\cos(\alpha d + \beta) + \gamma \tag{8}$$

where α, β, γ, and ω are the parameters to be solved. The above assumptions can be converted to the equations below:

$$\begin{cases} \omega\cos(\beta) + \gamma = 0 \\ \omega\cos(\alpha + \beta) + \gamma = 1 \\ -\alpha\omega\sin(\beta) = 0 \\ -\alpha\omega\sin(\alpha + \beta) = 0 \end{cases} \tag{9}$$

Assuming $w_l(d)$ is not a constant function, so $\alpha \neq 0$ and $\omega \neq 0$. Then:

$$\begin{cases} \alpha = \pi \\ \beta = 0 \\ \gamma = \frac{1}{2} \\ \omega = -\frac{1}{2} \end{cases} \tag{10}$$

We substitute (10) for (8), then $w_l(d)$ is derived:

$$w_l(d) = -\frac{1}{2}\cos(\pi d) + \frac{1}{2} \tag{11}$$

According to assumption (3), $w_r(d)$ is obtained by:

$$w_r(d) = 1 - w_l(d) = \frac{1}{2}\cos(\pi d) + \frac{1}{2} \tag{12}$$

To make an intuitive explanation of the weight variation, we provide a diagram showing how the weight varies with the distance ratio in Fig. 8. As shown in this figure, the weights w_l and w_r vary smoothly from 0 to 1, which meets our requirements in

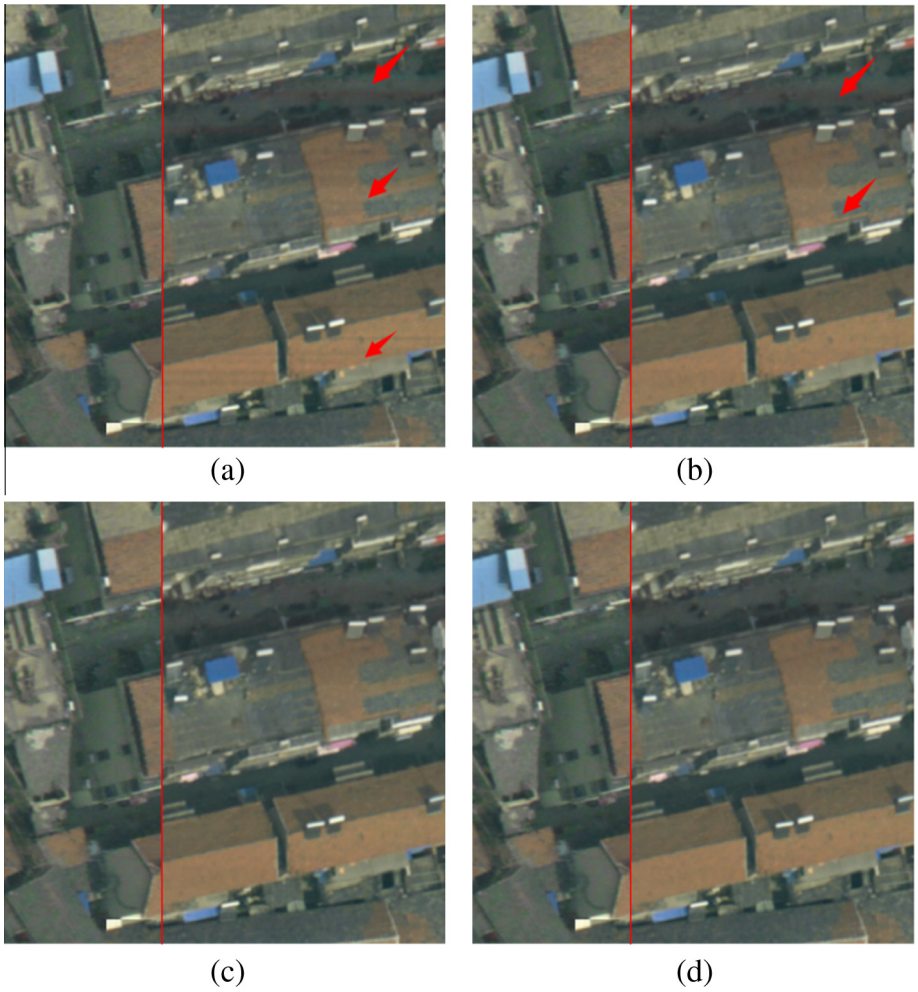

Fig. 11. Tonal adjustment results of LMM with different sizes of region [$2R+1$ in Eq. (2)]. (a) The result of $R=1$. (b) The result of $R=5$. (c) The result of $R=10$. (d) The result of $R=15$.

this sense. In general, a small value of q corresponds to an unnatural transition from one side to the other side of the detected seamline. When q is larger than 10, the blending effect is satisfactory. The larger the value of q, the smoother the transition.

4. Experiments and analysis

A number of experiments were conducted to validate the proposed method. Briefly speaking, the experiments were divided into three parts (the same as the previous content): tonal adjustment, seamline detection, and image blending. For airborne image examples, it is assumed that two pieces of images are taken when the focal plane is parallel. In the experiments, without any special instructions, the parameters for the proposed method are set as Table 1. More details follow.

4.1. Tonal adjustment

The two images in Fig. 9 are the original data. They are aerial images from an urban area with a spatial resolution of 0.1 m. The buildings in the images are concentrated, with some high buildings being apparently oblique, and several main roads separate the street area into blocks. We can see that the two images have an obvious tonal difference, and the gray level of each band is in the range [0,255]. In the tonal adjustment experiments, we set the overlapped area of the left image to be the reference, and adjusted the tone of the right image using three methods: LSM, MM, and LMM, respectively.

Fig. 10 shows the tonal adjustment results, in which the two images are mosaicked along the borders of the left image. On the whole, as can be seen in Fig. 10, the result of LSM still has considerable differences after the tonal adjustment, and is clearly worse than the results of MM and LMM. This is because the aerial images were shot from different angles, and the pixels on the same geographic location on the overlapped area do not match with each other accurately. Furthermore, LSM, which is based on an inaccurate difference between the pixels in the same location, cannot adjust the tone effectively. From an overall perspective, the tones of the results of MM and LMM are similar to each other. However, on the borders of the overlapped area (red[2] box and green box zoomed-in areas, see Fig. 10(b) and (c)), the result of MM shows some tonal difference. This is because of the fact that in the framework of MM, only one pair of gain and bias values is shared by all the pixels of the adjusted image, and the regional differences are ignored. In contrast, for LMM, every row has an independent pair of gain and bias values on a sliding region with a fixed number of rows; as a result, the local features are made better use of at the

[2] For interpretation of color in Fig. 10, the reader is referred to the web version of this article.

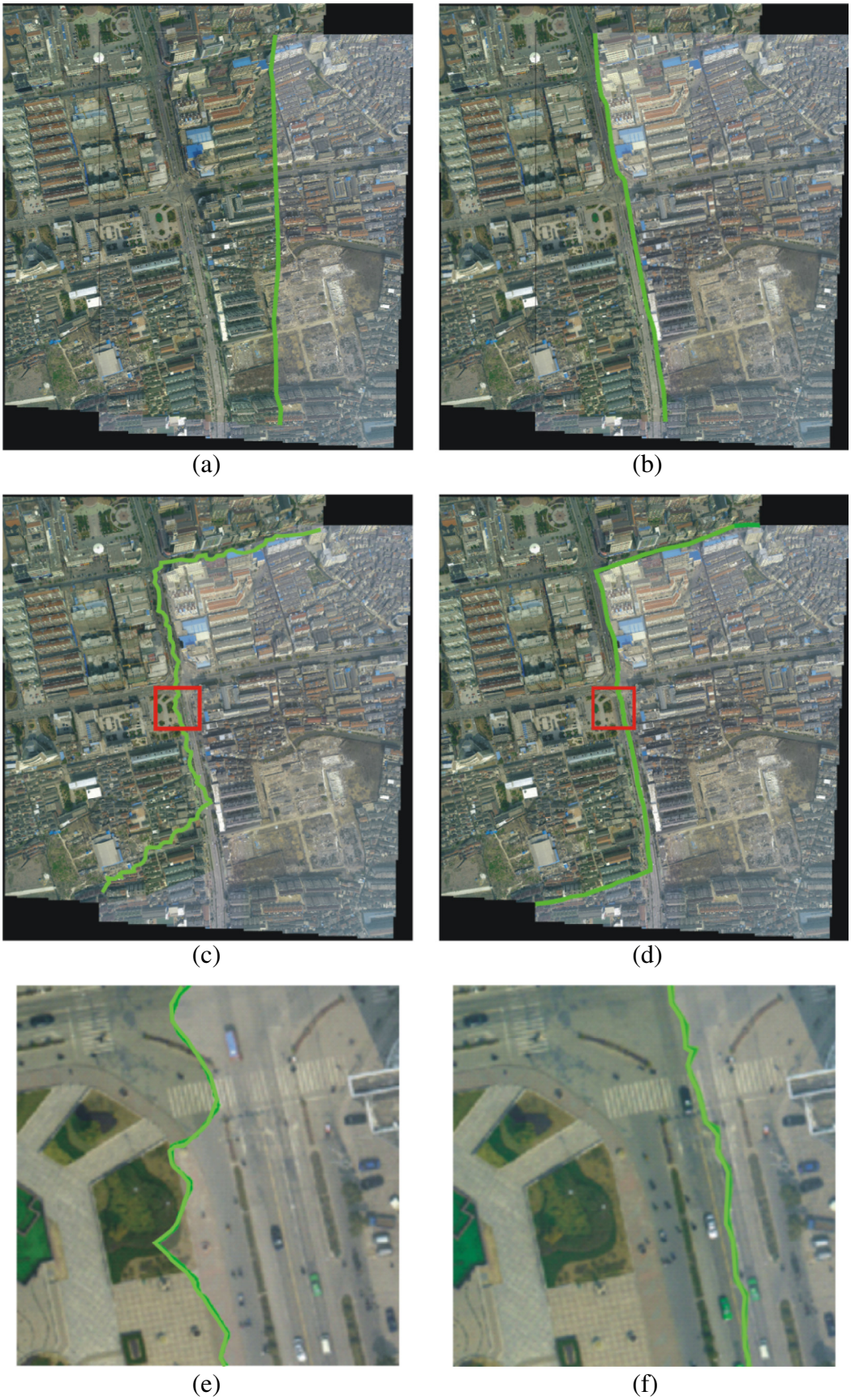

Fig. 12. Comparison of the seamline detection results by the use of the different methods. (a) The result of DP. (b) The result of APDP in the longitudinal direction. (c) The result of Inpho OrthoVista (software). (d) The result of the APDP final seamline. (e) and (f) The zoomed-in red boxes in (c) and (d). (For interpretation of the references to colour in this figure legend, the reader is referred to the web version of this article.)

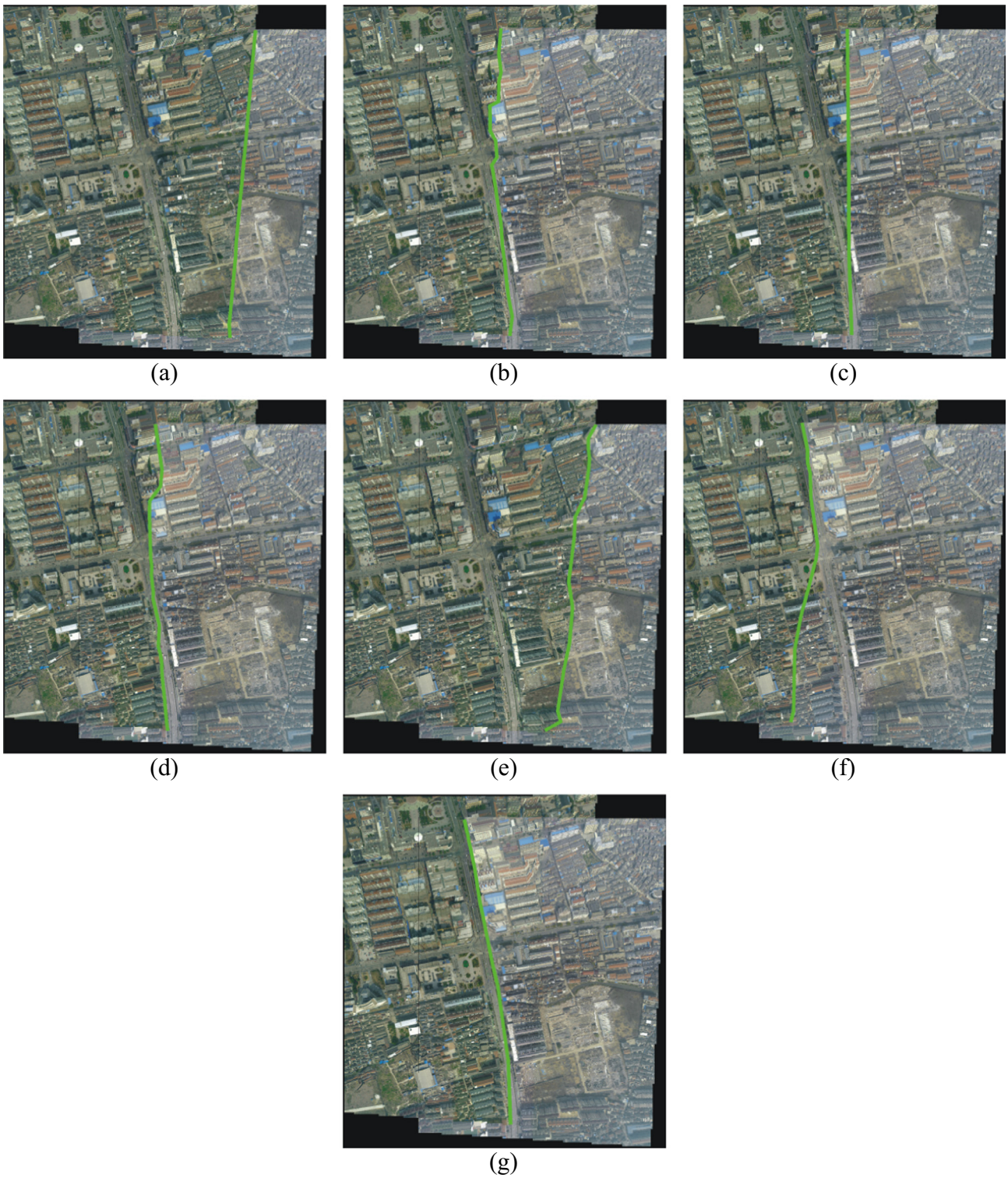

Fig. 13. Seamline detection results with different combinations of the different terms in expression (3) (without tonal adjustment). (a) The result of N_{dmk}. (b) The result of N_{emk}. (c) The result of N_{gmk}. (d) The result of $N_{dmk} + N_{emk}$. (e) The result of $N_{dmk} + N_{gmk}$. (f) The result of $N_{emk} + N_{gmk}$. (g) The result of $N_{dmk} + N_{emk} + N_{gmk}$.

regional level. This experiment demonstrates that LMM performs effectively for the tonal adjustment.

In order to quantitatively evaluate the effect of the tonal adjustment in Fig. 10, we consider the horizontal gradient at the color transition line (the blue line in Fig. 10(a)) of the two images as the indicator. For Fig. 10(a), suppose that the right edge (blue line) of the left image is column J (for brevity, we assume that it is strictly vertical), the left image is g, and the right image is f (the same as before), then the horizontal gradient ∇_x at the blue line is calculated by:

$$\nabla_x = \sum_i \nabla_x(i,J) = \sum_i |f(i,J+1) - g(i,J)| \tag{13}$$

A lower ∇_x means a smaller color difference, which corresponds to a better tonal effect. Since the images have red, green, and blue bands, we show the horizontal gradient at the color transition of

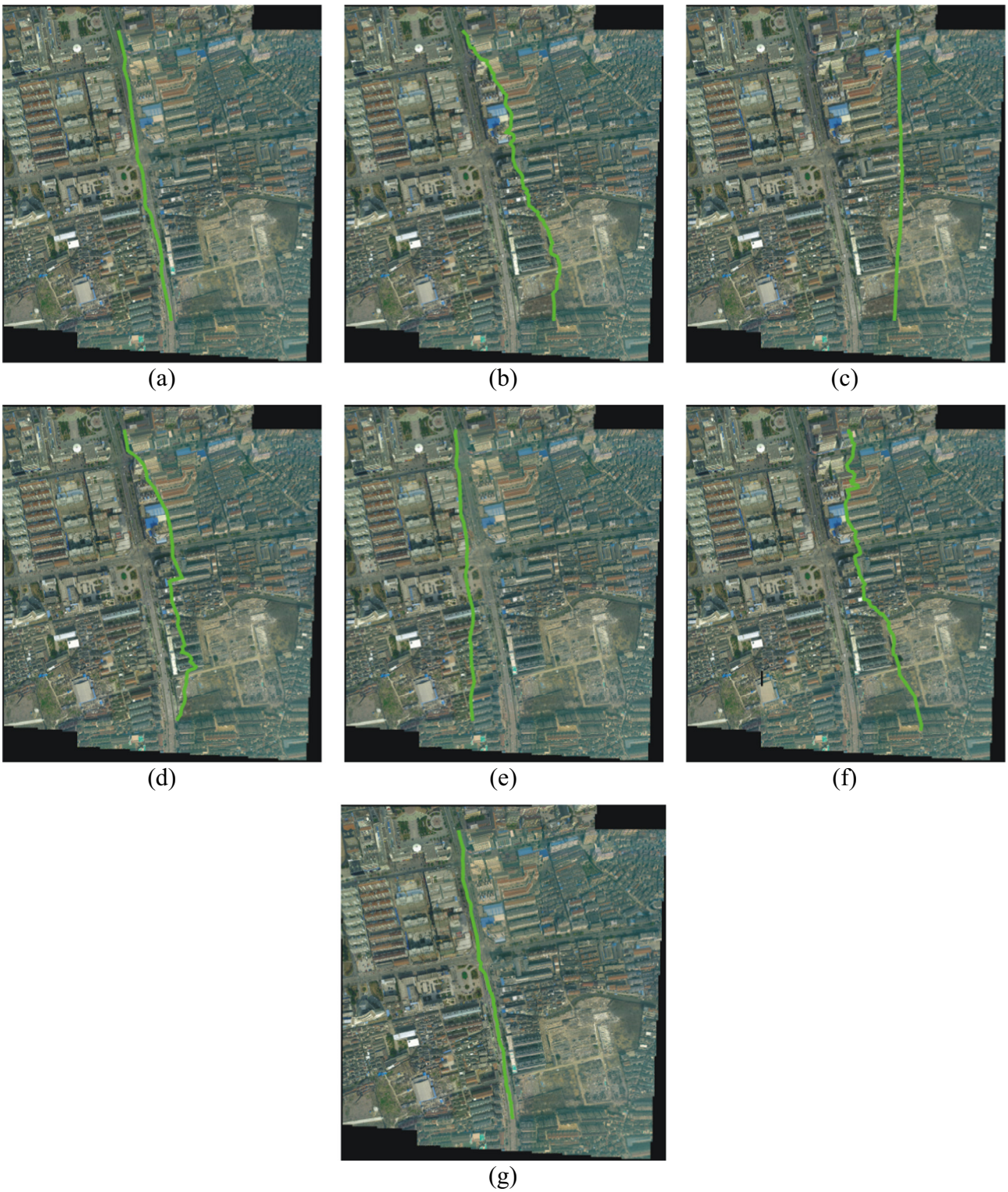

Fig. 14. Seamline detection results with different combinations of the different terms in expression (3) (with tonal adjustment by LMM). (a) The result of N_{dmk}. (b) The result of N_{emk}. (c) The result of N_{gmk}. (d) The result of $N_{dmk} + N_{emk}$. (e) The result of $N_{dmk} + N_{gmk}$. (f) The result of $N_{emk} + N_{gmk}$. (g) The result of $N_{dmk} + N_{emk} + N_{gmk}$.

each band in Table 2. As can be seen in Table 2, LMM obtains a lower horizontal gradient than LSM and MM, in keeping with the visual effect in Fig. 10. This experiment confirms that LMM obtains the best tonal adjustment among the three methods.

We then analyzed the influence of the region size of LMM on the tonal adjustment result. Fig. 11 shows the corrected results when the size of region changes in LMM. The original images are again Fig. 9. The red vertical line in Fig. 11 is the border of the left image. The section of the image on the left of the red line is inside the overlapped area, and the rest is outside the overlapped area. As shown in Fig. 11, when $R = 1$, the parts outside the overlapped area have very obvious horizontal strips, as shown by the red arrows. The strips are reduced when $R = 5$. Happily, when R is increased to 10, the strips disappear. When R is further increased to 15, it

Fig. 15. A poor seamline, with the seamline going through the building. The left image is the same as Fig. 14(b).

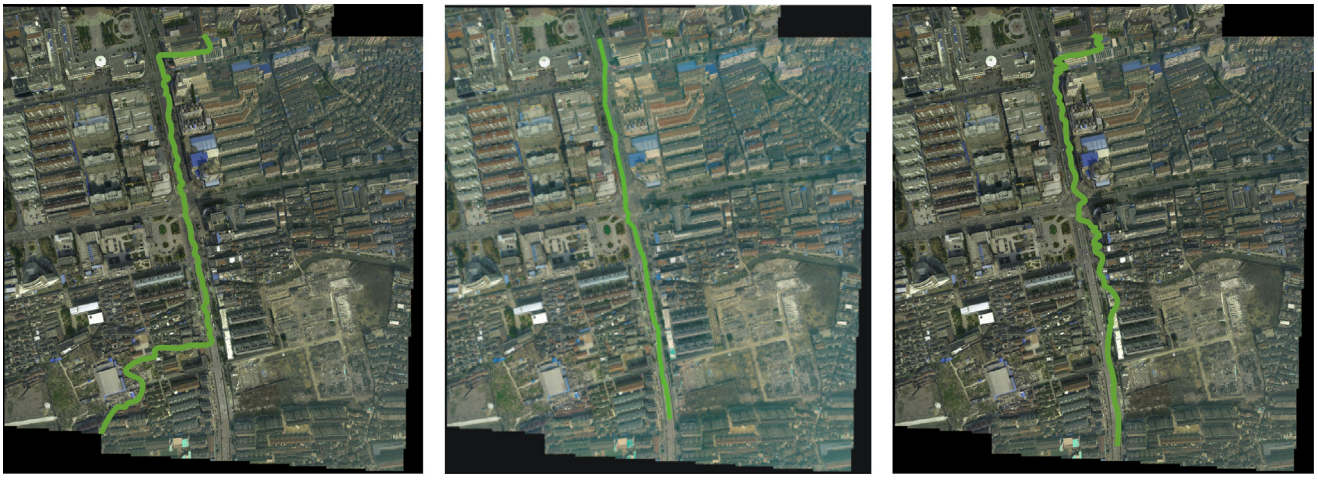

Fig. 16. Seamline detection results with different values of *TC*. (a) $TC = 200$. (b) $TC = 250$. (c) $TC = 300$.

does not show an obvious advantage over $R = 10$. This illustrates that, to a certain extent, a bigger region results in better tonal adjustment. Beyond this extent, it will not improve the visual appearance. The optimal size of region is also related to the amount of original data, the intensity difference of the neighboring images, and the degree of overlap. Generally and empirically, we have found that $R = 10$ is a good size and is suitable for a number of HR images.

4.2. Seamline detection

Mosaicking along the borders of the original images will generate great discontinuity. Similarly, a poor seamline will also cause this phenomenon. This is the reason why detecting an optimal seamline is important.

We undertook the following experiments: the first experiment was a comparison between the proposed method and the other existing methods; the second experiment analyzed how our algorithm affects the result of the seamline detection. Note that in the experiments, the cost threshold was set as $TC = 250$ and the length threshold was set as $TL = 100$.

Fig. 12 shows a comparison of the seamline detection results by the use of the different methods. Fig. 12(a) and (b) shows the difference between APDP and DP (Zagroub et al., 2009) in searching for the optimal seamline longitudinally, without tonal adjustment. Since DP does not adjust the tone, for a fair comparison, we did not conduct tonal adjustment in APDP. Moreover, DP only operates vertically; therefore, we did the same with APDP in this experiment. In Fig. 12(a) the seamline detected by DP goes almost vertically and crosses large areas of complex buildings, and can be considered to be a poor seamline according to the standards in Section 3.2. In other words, it cuts through buildings and causes discontinuities, which can be clearly observed when zooming in on the mosaicked image. In contrast, the longitudinal seamline found by APDP goes almost along the main road in Fig. 12(b). Along the road, the two images share the greatest similarity. Even though both images have different shooting angles, the areas on the road have the least difference. The comparison between Fig. 12 (a) and (b) shows that the discontinuity is alleviated by APDP to the greatest degree. This experiment indicates that APDP is an effective seamline detection method which gives rise to minimal discontinuity and dislocation.

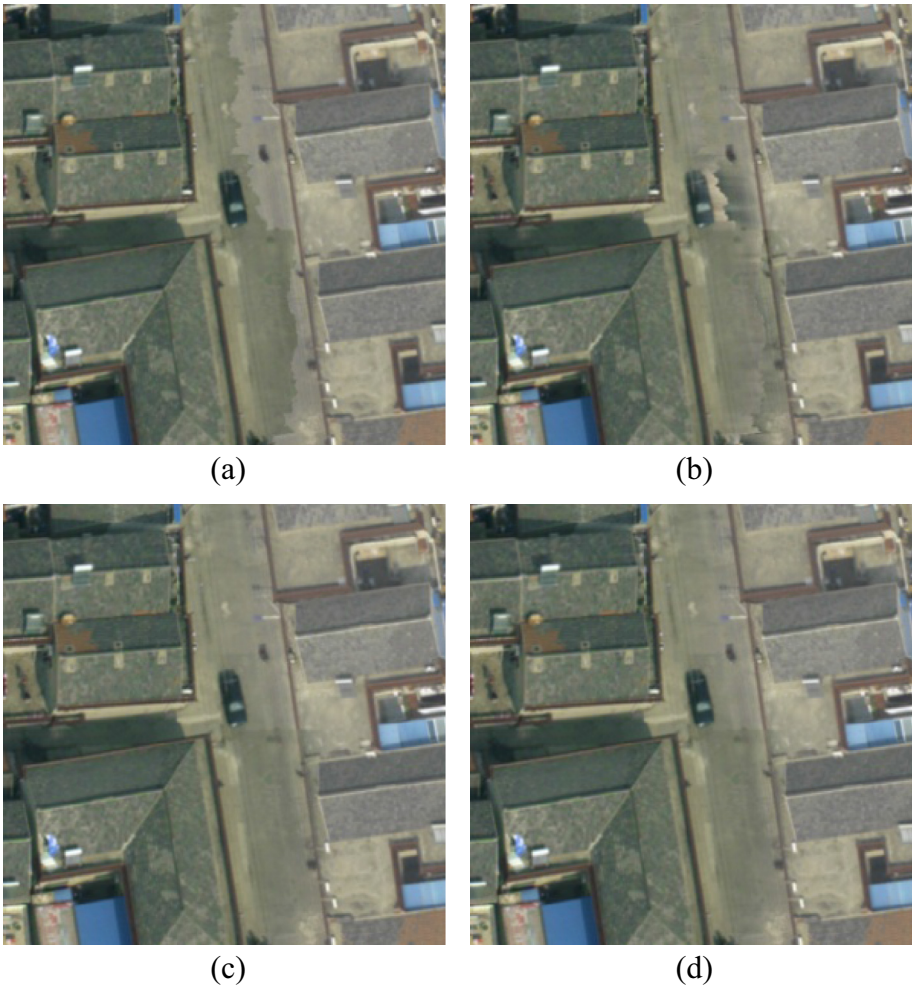

Fig. 17. Image blending using the different methods (without tonal adjustment). (a) The original. (b) The result of HC. (c) The result of IDW. (d) The result of the proposed CDWB.

Additionally, Fig. 12(c) and (d) compare the final integrated seamlines found by APDP and Inpho OrthoVista 4.5.0 (software, http://www.supermap.com.cn/inpho/download.asp). OrthoVista detects the seamline from the two vertexes of the overlapped area, and detects it not only vertically, which is very different from DP, so we did not compare them. On the whole, OrthoVista and APDP have similar visual results in Fig. 12(c) and (d). The careful reader will notice that the seamline detected by the proposed method goes roughly along the middle of the road, and the seamline detected by OrthoVista goes roughly along the edge of road (Fig. 12(e) and (f)). The optimal seamline benefits from two improvements: a piecewise detection method, and strict control of the optimal seamline. Therefore, APDP avoids the features on both sides of the road, and the discontinuities are reduced. Additionally, the seamline detected by OrthoVista often shows large fluctuations inside a small region. It is not as smooth, so that it increases the possibility of crossing into buildings. For example, in Fig. 12(e), the seamline gradually goes into the grassland beside the road. This experiment verifies that APDP detects a stable and pleasing seamline.

As shown previously, APDP is able to effectively detect the optimal seamline. We also undertook experiments to investigate how the algorithm ($N_{dmk}, N_{emk}, N_{gmk}$, and their different combinations) affects the location of the optimal seamline. To investigate the direct influence of APDP on the seamline, tonal adjustment was not applied to the images to be mosaicked. Fig. 13 shows the corresponding results of different combinations of N_{dmk}, N_{emk}, and N_{gmk}. A single N_{dmk}, N_{emk}, or N_{gmk} cannot obtain a good result, as shown in Fig. 13(a)–(c). Since the two images in this experiment have a large exposure difference, using N_{dmk} only, the seamline goes through the areas of similar exposure in Fig. 13(a). Fortunately the right-down part is a large area of flat ground, although without considering the geometric structure, the seamline tends to go through the area with the least tonal difference. N_{emk} (Fig. 13(b)) has a much better result than N_{dnk} (Fig. 13(a)) and N_{gmk} (Fig. 13(c)). However, in the first part, the seamline crosses through buildings. Using $N_{dmk} + N_{emk}$ (Fig. 13(d)) and $N_{emk} + N_{gmk}$ (Fig. 13(f)) obtains relatively better seamlines than $N_{dmk} + N_{gmk}$ (Fig. 13(e)), and the two seamlines mainly go along the road. Concretely, in Fig. 13(f), the start of the seamline lies in the middle of the road, and in Fig. 13(d), the seamline keeps going along the road, which is a pleasing result. Fig. 13(g) with $N_{dmk} + N_{emk} + N_{gmk}$, which combines the advantages of the methods used in Fig. 13(d) and (f), shows the best result. This experiment demonstrates that even if there are apparent tonal differences in the images, APDP is effective in detecting the optimal seamline in images of urban areas.

We also investigated how N_{dmk}, N_{emk}, and N_{gmk} and their different combinations affect the seamline detection after tonal adjustment. Fig. 14 shows the seamline detection results after tonal adjustment by LMM. Images after tonal adjustment have a similar

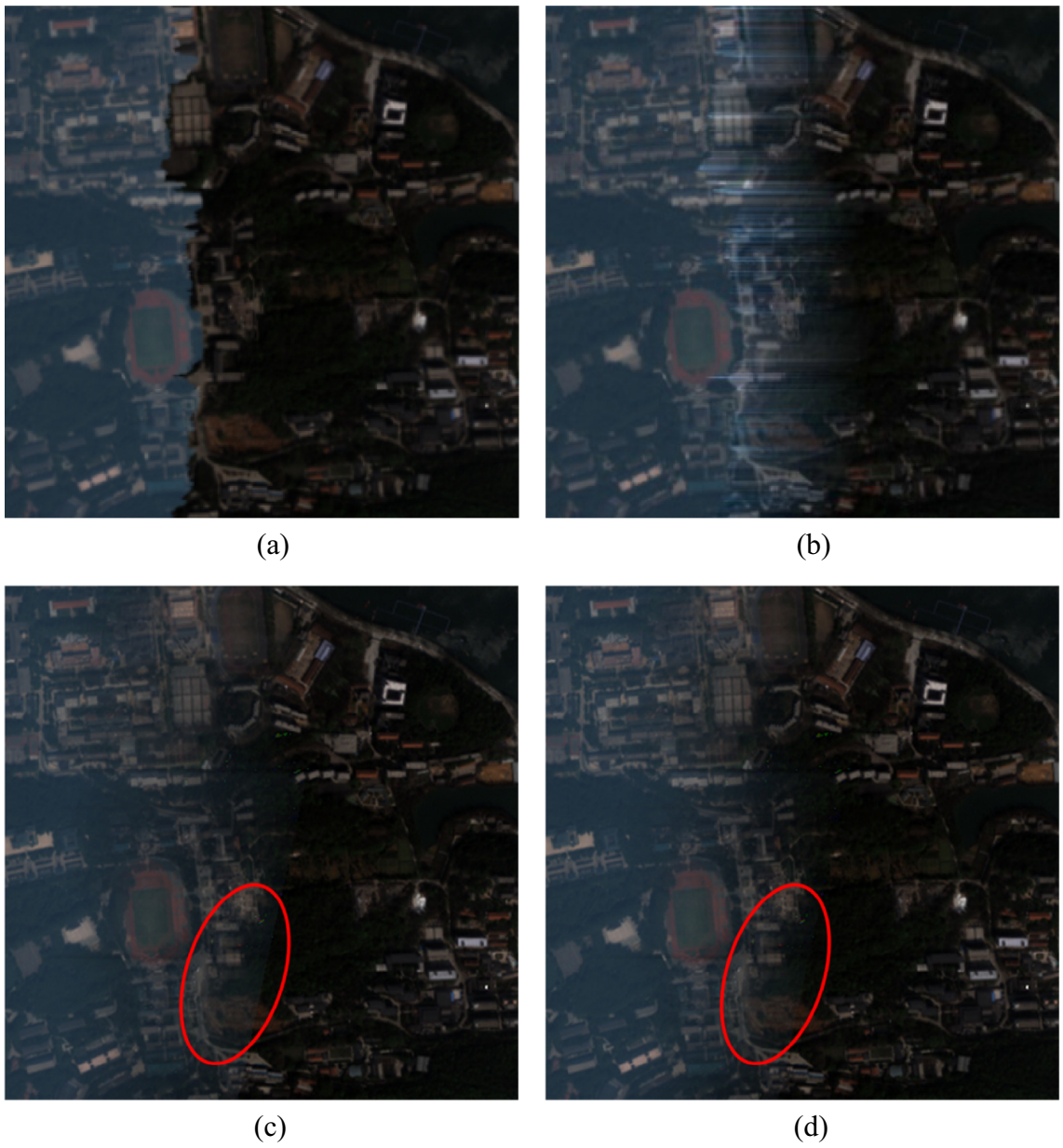

Fig. 18. Image blending using the different methods (without tonal adjustment) for QuickBird images. (a) The original. (b) The result of HC. (c) The result of IDW. (d) The result of the proposed CDWB.

intensity, especially in the flat areas, and the two original images are more similar. Thus, N_{dmk} (Fig. 14(a)) can obtain pleasing results. The seamlines in the other images fail to go along the main road. N_{gmk} (Fig. 14(c)) in particular detects a seamline that is almost vertical, similar to Fig. 13(c). Using $N_{dmk} + N_{emk} + N_{gmk}$, the seamline can correctly go along the road. Comparing Figs. 13(g) and 14(g), we see that after tonal adjustment, the detected seamline changes from going along the edge of the buildings, or going through the buildings, to going along the center of the road. This indicates that the tonal adjustment is very useful for the seamline detection.

From the results of the two experiments depicted in Figs. 13 and 14, we can see that no matter whether the images have a similar tone or not, $N_{dmk} + N_{emk} + N_{gmk}$ detects the optimal seamline in urban areas. Comparing Fig. 13(g) and 14(g), although the two seamlines both go along the road (which can be considered as satisfactory detection), when we zoom in on the neighborhood area of the seamline, it can be seen that the seamline in Fig. 13(g) partly goes into the buildings. When tonal adjustment is adopted, this phenomenon is avoided. As a result, we can conclude that the tonal adjustment is beneficial to the seamline detection. Additionally, it also demonstrates that the proposed procedure is reasonable.

Here, we reiterate that the seamline detection is the key step in the proposed procedure. For the HR images of an urban area, the same building on two images acquired from different times will have an obvious inclination difference. This kind of difference can result in a mismatch. We show an example of poor seamline detection in Fig. 15, in which the seamline goes through the building. In this situation, no matter how effective the tonal adjustment and blending, the discontinuity along the seamline will be kept in the final mosaicking result.

We now discuss how different values of TC affect the seamline detection. Fig. 16 shows the detection results. As shown in Fig. 16, when $TC = 200$, the seamline goes through the buildings, which is considered as a poor seamline in HR images. Similarly, when

Fig. 19. Image blending using CDWB with/without LMM. (a) The result without LMM. (b) The result with LMM.

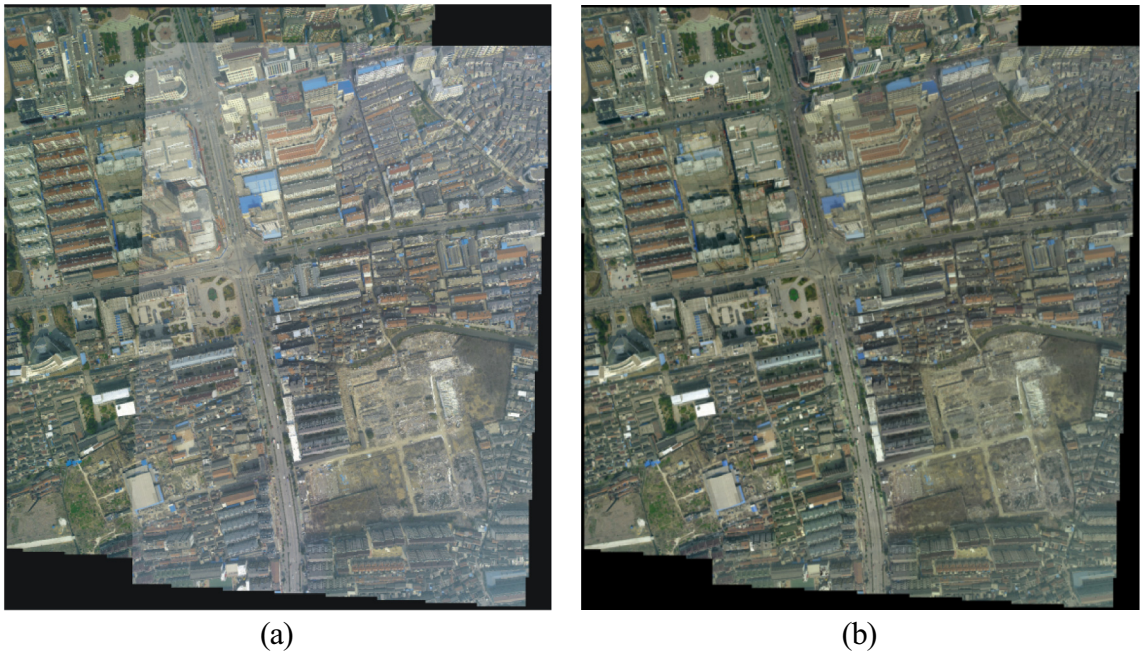

Fig. 20. Mosaicked results of 0.1-m resolution aerial images. (a) Original images along the borders (original). (b) The mosaicked result of the proposed method.

$TC = 300$, the seamline also partly goes into the buildings. However, when $TC = 250$, the seamline goes along the road. This experiment demonstrates that a moderate value of TC obtains a satisfactory effect. As stated in the algorithm section, TC is a threshold added by N_d, N_g, and N_e, which controls the selection of the optimal seamline. However, TC is correlated with the geographical features. A mechanism for the adaptive selection of TC will be determined in the future.

4.3. Image blending

We also tested three different approaches to eliminating the seamline (for comparison): HC, IDW, and the proposed CDWB. Note that in the complete process of our mosaicking method, the image blending is the final step (after tonal adjustment and seamline detection). In the experiments, the half width of the buffer $q = 10$. To evaluate the direct effects of the image blending by the use of the three methods, we first show the results generated without tonal adjustment (Fig. 17). The original image without tonal adjustment has an obvious seamline in Fig. 17(a). HC does not eliminate the seamline very well in Fig. 17(b); it corrects the intensity difference by calculating the intensity on the two sides of the seamline, respectively, and then averages the difference between the two sides based on the distance weight. The result, however, is no better than the overlapping methods (Fig. 17 (c) and (d)). IDW (Fig. 17(c)) and CDWB (Fig. 17(d)) successfully

Fig. 21. Mosaicked results of 2.6-m resolution QuickBird images. (a) Original images along the borders (original). (b) The mosaicked result of the proposed method.

eliminate the seamline. In this case, CDWB does not show any advantage over IDW, because the tones of the original images are very similar.

We also undertook another mosaicking experiment with QuickBird (HR) images to further show the differences between these elimination methods. Fig. 18(a) is the original result without blending. After HC processing, there is still an obvious seamline in Fig. 18(b). In Fig. 18(c) and (d), the intensity gradually changes from the left image to the right one. However, without tonal adjustment, the seamline can be eliminated to a certain degree. As shown in the red circled areas, the transition by CDWB near the borders of the buffer is smoother than for IDW. This experiment verifies that CDWB is better than IDW when the tonal difference is obvious.

In the complete mosaicking process (with tonal adjustment by LMM), we tested how effectively the seamline was eliminated by the three methods. The images in Fig. 19, zoomed in from Fig. 18, show the CDWB results with and without tonal adjustment. Fig. 19(a) shows the result of directly eliminating the seamline without tonal adjustment. Fig. 19(b) shows the result after using LMM to adjust the tone. After tonal adjustment, the mosaicked images have a quite close intensity. Using CDWB with LMM, the seamline is eliminated and the mosaicked image is a seamless mosaic.

4.4. Final mosaicked results

Fig. 20 is the final mosaicked image generated from two aerial images, with tonal adjustment (LMM), seamline detection (APDP), and image blending (CDWB). The results show a stable brightness, and there is no apparent trace of a seamline. Fig. 21 is the mosaicked image of the QuickBird satellite images (the images in Figs. 18 and 19 are cropped from them). As shown in these figures, the proposed method successfully generates a seamless mosaic. Furthermore, aerial images are shot close to the ground, which means that the images have more obvious deformations than satellite images. In other words, continuous satellite images will have more similarities in the overlapped area, and the mosaicked results will be more pleasing. Overall, the experiments proved that the proposed mosaicking procedure and algorithms are effective.

5. Conclusions and discussions

This paper has proposed three improvements in the procedure of HR image mosaicking. In the first step—tonal adjustment—we use LMM to correct the tonal difference. LMM successfully takes the local tonal characteristics into account and makes the images uniform in tone. Then, in the second step—seamline detection—a piecewise detection method, APDP, is proposed to determine the location of the optimal seamline, which avoids the seamline passing through buildings by ending the current detection once beyond the threshold. That is, APDP finds the optimal seamline in the flattest area or along the natural edges of buildings. After that, in the final step—image blending—CDWB is used to blend the buffer along the optimal seamline, and realizes a perfect cosine curve smoothly from one image to the other. All these operations together result in an invisible seamline. The three improvements all result in a good visual effect and are appropriate for large amounts of data. According to the experiments, it was found that the seamline detection is the key step in the proposed procedure. The tonal adjustment is also conducive to the subsequent seamline detection.

The proposed mosaicking procedure is applicable for both aerial photographs and HR satellite images. However, there is still room for improvement. LMM is not very effective for images with a very small overlapped area. In addition, a mechanism for the adaptive selection of the *TC* threshold of APDP will be investigated in the future. The proposed method is, however, suitable for the mosaicking of multiple HR images one after another. For the convenience of description, we just used the mosaicking of two HR images as an example in the experiments. The simultaneous mosaicking of multiple HR images will be in our future research focus. Another point should be noted that for the airborne image experiments, we assumed the images to be mosaicked are acquired with the parallel focal plane. In this condition, the geometric distortion is not notable. However, once the aerial platform randomly moves,

the geometric distortion is usually so huge that our method doesn't directly work. If the images are effectively exerted on geometric correction, maybe our method is back to life. When remote sensing images are covered by clouds, the clouds should be removed before mosaicking (Shen et al., 2015). Additionally, maybe the variational method (Shen et al.) can be applied in this field in the future.

Acknowledgments

This work was supported by the National Natural Science Foundation of China (NSFC) under Grant No. 41422108, the Program for Changjiang Scholars and Innovative Research Team in University under Grant IRT1278, and the Fundamental Research Funds for the Central Universities of China under Grant Nos. 2042014kf0199, 2042014kf0299, and 2014205020201. The authors would also like to thank the anonymous reviewers.

References

Agrawal, H., Horgan, J.R., 1990. Dynamic program slicing. In: ACM SIGPLAN'90 Conference on Programming Language Design and Implementation, New York, USA. pp. 246–256.

Burt, P.J., Adelson, E.H., 1983. A multiresolution spline with application to image mosaics. ACM Transact. Graph. 2 (4), 217–236.

Chon, J., Kim, H., 2006. Determination of the optimal seam-lines in image mosaicking with the dynamic programming (DP) on the converted cost space. In: the 8th International Conference on Artificial Intelligence and Soft Computing (ICAISC), Zakopane, Poland. pp. 750–757.

Davis, J., 1998. Mosaics of scenes with moving objects. In: IEEE Computer Society Conference on Computer Vision and Pattern Recognition (CVPR), Santa Barbara, USA. pp. 354–360.

Dijkstra, E.W., 1959. A note on two problems in connection with graphs. Numer. Math. 1 (1), 269–271.

Du, Y., Cihlar, J., Beaubien, J., Latifovic, R., 2001. Radiometric normalization, compositing, and quality control for satellite high resolution image mosaics over large areas. IEEE Trans. Geosci. Remote Sens. 39 (3), 623–634.

Duplaquet, M.-L., 1998. Building large image mosaics with invisible seam-lines. In The SPIE Conference on Visual Information Processing, Orlando, USA. pp. 369–377.

Fisher, N.I., Lewis, T., Embleton, B.J.J., 1987. Statistical Analysis of Spherical Data. Cambridge University Press, Cambridge, p. 329.

Gonzalez, R.C., Woods, R.E., 2007. Digital Image Processing, fourth ed. Publishing House of Electronics Industry, Beijing.

Kang, Y.-K., 2006. Image information processing system. IJCSNS Int. J. Comput. Sci. Network Security 6 (12), 128–137.

Kass, M., Witkin, A., Terzopoulos, D., 1988. Snakes: active contour models. Int. J. Comput. Vision 1 (4), 321–331.

Kerschner, M., 2000. Twin snakes for determining seam lines in orthoimage mosaicking. Int. Arch. Photogr. Remote Sens. 33 (4), 454–461.

Kerschner, M., 2001. Seamline detection in colour orthoimage mosaicking by use of twin snakes. ISPRS J. Photogr. Remote Sens. 56 (1), 53–64.

Levin, A., Zomet, A., Peleg, S., Weiss, Y., 2004. Seamless Image Stitching in the Gradient Domain. Computer Vision-ECCV 2004. Springer, pp. 377–389.

Mills, A., Dudek, G., 2009. Image stitching with dynamic elements. Image Vis. Comput. 27 (10), 1593–1602.

Pan, J., Wang, M., Li, D., Li, J., 2009. Automatic generation of seamline network using area voronoi diagrams with overlap. IEEE Trans. Geosci. Remote Sens. 47 (6), 1737–1744.

Pham, B., Pringle, G., 1995. Color correction for an image sequence. IEEE Comput. Graphics Appl. 15 (3), 38–42.

Shen, H., Li, X., Cheng, Q., Zeng, C., Yang, G., Li, H., Zhang, L., 2015. Missing information reconstruction of remote sensing data: a technical review. IEEE Geosci. Remote Sens. Mag. 3 (3), 61–85.

Shen, H., Peng, L., Yue, L., Yuan, Q., Zhang, L. Adaptive Norm Selection for Regularized Image Restoration and Super-Resolution", IEEE Transactions on Cybernetics, http://dx.doi.org/10.1109/TCYB.2015.2446755.

Shmuel, P., 1981. Elimination of seams from photomosaics. Comput. Graph. Image Process. 16 (1), 90–94.

Uyttendaele, M., Eden, A., Szeliski, R., 2001. Eliminating ghosting and exposure artifacts in image mosaics. In: IEEE Computer Society Conference on Computer Vision and Pattern Recognition (CVPR), Kauai, USA. pp. II-509–II-516.

Wang, L., Ai, H., Zhang, L., 2010. Automated seamline detection in orthophoto mosaicking using improved snakes. In: The 2nd International Conference on Information Engineering and Computer Science (ICIECS), Wuhan, China. pp. 1–4.

Xing, C., Wang, J., Xu, Y., 2010. An optimal seamline based mosaic method for UAV sequence images. In: The International Conference on Civil and Environmental Engineering (ICCEE), Rio de Janeiro, Brazil.

Yi, Y., Gong, J., Qin, Q., 2003. Hue adjustment method of large-scale image database. Geomat. Inform. Sci. Wuhan Univ. 28 (3), 311–314 (in Chinese).

Zagroub, E., Barhoumi, W., Amri, S., 2009. An efficient image-mosaicing method based on multifeature matching. Mach. Vis. Appl. 20 (3), 139–162.

Zhang, Z., Li, Z., Zhang, J., Li, Z., 2003. Use discrete chromatic space to tune the image tone in color image mosaic. In: The 3rd International Symposium on Multispectral Image Processing and Pattern Recognition, Beijing, China. pp. 16–21.

Zhong, Y., Liu, L., Wang, J., Yan, G., 2006. A method based on moment matching algorithm to correct remotely sensed image in rugged area. Geogr. Geoinform. Sci. 22 (1) (in Chinese).

Zhu, S., Qian, Z., 2002. The seam-line removal under mosaicking of remotely sensed images. J. Remote Sens. 6 (3), 183–187 (in Chinese).